remote sensing

MDPI

Article

Post-Hurricane Debris and Community Flood Damage Assessment Using Aerial Imagery

Diksha Aggarwal [1], Suyog Gautam [2], Daniel Whitehurst [1] and Kevin Kochersberger [1,*]

[1] Department of Mechanical Engineering, Virginia Tech, Blacksburg, VA 24061, USA; diksha@vt.edu (D.A.); dsw418@vt.edu (D.W.)
[2] Department of Geography, Virginia Tech, Blacksburg, VA 24061, USA; suyoggtm@vt.edu
* Correspondence: kbk@vt.edu

Highlights

What are the main findings?

- Using a combination of machine learning and non-machine learning tools on aerial imagery to provide rapid estimation of debris in lakes, land, and near streams, with accuracy sufficient for preliminary disaster assessments.
- Flood modeling can be used to rapidly assess damage in a community with limited ground truth data, with errors less than 8% demonstrated for a small Appalachian community.

What is the implication of the main finding?

- Proposed methods for debris estimation from aerial imagery offer more efficient alternatives to slow, labor-intensive visual inspection and ground-based methods, improving the timeliness and accuracy of recovery planning.
- Validated flood modeling can support proactive community-level damage classification before field surveys, accelerating disaster response decisions.

Abstract

Natural disasters often result in significant damage to infrastructure, generating vast amounts of debris in towns and water bodies. Timely post-disaster damage assessment is critical for enabling swift cleanup and recovery efforts. This study presents a combination of methods to efficiently estimate and analyze debris on land and on water. Specifically, analyses were conducted at Claytor Lake and Damascus, Virginia where flooding occurred as a result of Hurricane Helene on 27 September 2024. We use the Phoenix U15 motor glider equipped with the GoPro Hero 9 camera to collect aerial imagery. Orthomosaic images and 3D maps are generated using OpenDroneMap (ODM) software, version 3.5.6, providing a detailed view of the affected areas. For lake debris estimation, we employ a hybrid approach integrating machine learning-based tools and traditional techniques. Lake regions are isolated using segmentation methods, and the debris area is estimated through a combination of color thresholding and edge detection. The debris is classified based on the thickness and a volume range of debris is presented based on the data provided by the Virginia Department of Environmental Quality (VDEQ). In Damascus, debris estimation is achieved by comparing pre-disaster LiDAR data (2016) with post-disaster 3D ODM data. Furthermore, we conduct flood modeling using the Hydrologic Engineering Center's River Analysis System (HEC-RAS) to simulate disaster impacts, estimate the flood water depth, and support urban planning efforts. The proposed methodology demonstrates the ability to deliver accurate debris estimates in a time-sensitive manner, providing valuable insights for disaster management and environmental recovery initiatives.

Academic Editor: A. K. M. Azad Hossain

Received: 11 June 2025
Revised: 18 August 2025
Accepted: 5 September 2025
Published: 12 September 2025

Citation: Aggarwal, D.; Gautam, S.; Whitehurst, D.; Kochersberger, K. Post-Hurricane Debris and Community Flood Damage Assessment Using Aerial Imagery. *Remote Sens.* **2025**, *17*, 3171. https://doi.org/10.3390/rs17183171

Keywords: drones; aircraft; hurricane; flood; debris; segmentation; flood modeling; emergency response; damage assessment; 3D point cloud; lakes; streams

1. Introduction

Time-sensitive and accurate data collection and analysis after a major flood event is critical to reducing the impact on lives and livelihoods. The initial response to a flood event is directed at saving lives and assessing overall damage, usually through a combination of ground-based and aerial search-and-rescue activities. If this initial response occurs within the first two days, then the next phase lasts several weeks and is directed at a more detailed assessment of damage to help plan for a longer-term recovery effort.

National responding agencies such as the U.S. Army Corps of Engineers (USACE), Federal Emergency Management Agency (FEMA), and the Natural Resources Conservation Service (NRCS) are heavily engaged in damage assessment and planning to restore natural and built environments that have been altered by a flood [1]. State agencies and local governments are also engaged in this work, usually in coordination with the national agencies to share data and recovery plans and commit to recovery activities. The planning for large-scale recovery must happen efficiently and accurately since response delays have been shown to amplify public skepticism and concerns about what is actually happening on the ground [2,3]. Delayed response also leads to a lower QALY, which is the quality-adjusted life years [4,5]. A lower QALY is the result of psychological trauma and depression that is faced by the victims in a disaster. Therefore, the rapid acquisition of ground truth and subsequent accurate estimates of damage and recovery effort are needed now more than ever.

Efforts have been made by several researchers in the direction of obtaining accurate estimates of damage. Damage estimation starts with the process of collecting the data from the regions impacted by disasters. Uncrewed Aerial Vehicles (UAVs) have become an accepted means of data collection and monitoring by public safety and first responders who are on-site and need actionable data fast. Authors have also explored the use of UAVs in post-disaster assessment. Sakurada et al. [6] demonstrated this by merging street view and aerial view data to estimate the debris in the city after the Tsunami in the city of Kamaishi, Japan. Ghaffarian et al. [7] combined satellite and UAV images to identify debris, leveraging their complementary perspectives and resolutions. Satellite data is useful in large area surveys; however, there can be delays due to weather and scheduling. UAVs are instrumental when the observed area is geometrically small. A single operator can fly the aircraft over a scene and maintain visual line-of-sight while maneuvering over areas that cannot be viewed on the ground, thus providing a bird's-eye perspective of the area under consideration. Relevant research is discussed below, with a summary of comparison of different platforms and techniques presented in Table 1.

Table 1. Comparative analysis of existing methods for post-disaster debris and flood assessment.

Method	Data Type	Technique	Advantages	Limitations
Sakurada et al. (2016) [6]	Aerial + Street View	Random Forest Regressor for debris probability mapping	High spatial detail; improved context awareness	Dataset dependent; low absolute precision
Ghaffarian et al. (2019) [7]	Satellite + UAV	Textural features and HOG analysis to classify debris	Highlights overestimation risk in damage assessments	No classification or quantitative accuracy reported

Table 1. *Cont.*

Method	Data Type	Technique	Advantages	Limitations
Madkour et al. (2022) [8]	UAV	DeepLabV3 segmentation + color thresholding	High segmentation accuracy (97.8%)	High computation cost; needs custom training
Celik (2009) [9]	Satellite	PCA + k-means clustering for change detection	No training needed; fast processing	Requires pre-disaster images; No labeling of change detected
Simantiris et al. (2024) [10]	UAV	LAB color space + RGB Vegetation Index + edge detection	Simple rule-based segmentation; good for open areas	Not robust to thick debris layers; limited generalizability
Tamin et al. (2019) [11]	UAV	Photogrammetry for volume estimation	High accuracy in volume estimates; low-cost UAV-based solution	Needs unobstructed surface; not applied to disaster cases
Proposed Method (This Study)	Motorglider	Photogrammetry + Segmentation + color thresholding + edge detection + HEC-RAS	Rapid and low-cost; flood modeling and debris estimation; minimal setup	Lacks automation in debris labeling

UAVs are generally classified into Fixed-Wing and VTOL (Vertical Take-Off and Landing) based on aerodynamic design and flight characteristics. Fixed-wing aircraft have range advantages over VTOL aircraft and are suitable for large-area surveys; however, in the case of drones, FAA authorization is currently required for any remotely piloted aircraft flying beyond visual line-of-sight [12]. Crewed aircraft then become a feasible imaging solution for large-scale data collection campaigns, and we demonstrate that a fuel-efficient motorglider using a consumer-grade camera can collect tens of square miles of good-quality imagery in a single flight, at low cost.

Debris in lakes present a health and safety risk since lakes are frequently a source of potable water for communities and also provide recreational opportunities through watersports. This debris can consist of natural products such as trees and vegetative matter and man-made items that were damaged or deposited due to high water levels or high flow velocity. Removing debris in lakes is a high priority, and obtaining an estimate of debris coverage is the first step required to allocate funds for contract work. These estimates have historically been completed visually, either from a boat or plane, and relatively simple rules are applied to estimate debris volume [1]. These estimates can be significantly wrong using visual methods. With advances in remote sensing, debris can be further classified into density grades, which enables more accurate debris analysis and estimation, supporting more effective disaster management.

A key aspect of this process is segmentation, which involves partitioning images into meaningful regions, such as separating water, debris, and land from each other. Segmentation is essential for quantifying debris coverage and understanding its distribution. Two approaches exist for segmentation: machine learning- and non-machine learning-based methods. Machine learning methods involve training a model on a dataset of images labeled with the object of interest to perform required operations on images. Datasets like RescueNet [13] and FloodNet [14] offer high-resolution UAV imagery tailored for segmenting water, flooded infrastructure, and vegetation. Nugraha et al. [15] utilized FloodNet to train deep convolutional neural networks (CNN) like U-Net and PSPNet on aerial imagery from UAV. These CNNs perform semantic segmentation on the images by categorizing image parts that belong to the same class, achieving good accuracy. However, these datasets do not involve debris in water. Therefore, Madkour et al. [8] trained the

DeepLabV3 model on their own dataset and performed segmentation. They achieved a validation accuracy of 97.8% with the training time of nearly 97 min on a machine with significant computational resources for the implementation. Machine learning methods, while effective, are resource intensive and take a considerable amount of time to set up, train, and fine-tune a model.

As an alternative, researchers have also explored non-machine learning-based methods. Celik [9] developed an unsupervised change detection method by image differencing and using PCA analysis and k-means clustering on multitemporal satellite images. Change detection provides good results if the images of the required region are available before and after the disaster. Before a disaster, the main source of imagery can be only satellites. Acquiring such satellite images in high quality takes a lot of time and might not be feasible for all regions. Simantiris et al. [10] proposed the detection of non-flooded areas from UAV images utilizing masks over the LAB colorspace, and RGB vegetation index and edge detection on the original RGB image. The model performed considerably well on several datasets; however, it did not outperform deep learning-based methods. Additionally, this method may not perform well if water has a thick debris layer floating on it, as it will be difficult to segment debris from the non-flooded areas. Madkour et al. [8] performed the segmentation of land and water using machine learning and utilized color thresholding in water to further segment the debris layer. They provided an estimation of the area of debris in water, but they did not classify the debris based on thickness and density that can give a volume estimation of the debris and compare with the ground measurements. Accurate ground measurements are available typically after the clean-up activity when the debris is measured at the landfill gate based on the capacity of the truck beds [16]. The literature lacks methods that correlate these measurements with the area of the affected region covered with the debris.

On land, there is still a requirement to find debris, but the problem becomes three-dimensional. Cleanup activities in communities require an analysis of displaced debris. Initiatives by the NRCS like the Emergency Watershed Program facilitate communities in removing debris from stream channels, road culverts, and bridges [17]. Past work by such programs to quantify the volume of material washed into waterways that subsequently create chokepoints has been accomplished using ground-based measurements only. Typically, trained personnel assess the volume and distribution of debris through visual inspections and measurements [18]. This information is then used to plan and prioritize debris-removal efforts to mitigate threats to life and property effectively. The actual removal of debris from waterways can take several years, as logistically it is a very challenging task to reach remote areas surrounded by developed land while minimizing the impact on the environment [19].

These efforts can be significantly reduced by using three-dimensional (3D) reconstruction techniques to generate point cloud and digital elevation models (DEMs) for estimating stockpile volume, which is a common application of photogrammetry. Researchers like Tamin et al. [11] and Mantey et al. [20] generated 3D point cloud data using UAV imagery and estimated the stockpile volume for the earthwork and achieved an error of 0.002% and 0.08%, respectively. To the author's knowledge, this philosophy has been widely discussed in surveying and mining and has not been implemented in debris estimation after a disaster.

Floodwater height modeling in communities has been performed in the past to assess flood risk, which includes water height estimate (for water inundation analysis) and hydrological flow analysis. Whitehurst et al. [21] employed HEC-RAS with post-flood DEM data to model a flood event. Their analysis predicted future floodwater height in the affected area under the scenario of a recurring flood event with the new debris deposit. Similarly, Sattar et al. [22] studied the 2016 Gongbatongsha Glacier Lake Outburst Flood by

employing HEC-RAS to model the hydrodynamic flood behavior and RAMMS to simulate the debris flow dynamics. They reconstructed the event, estimating flow discharge and debris entrainment. Elkhrachy [23] further trained different machine learning models for water depth prediction. The models use the input features from Synthetic Aperture Radar (SAR), DSM, and optimal imagery data after the flash flood in New Cairo City, Egypt, and correlate them with the water depth obtained from the HEC-RAS model. Flood water height can be used by agencies to estimate the damage caused in buildings.

In our work, two areas affected by Hurricane Helene in Southwest Virginia were studied to develop the means of obtaining higher accuracy estimates of damage than what has previously been possible to achieve. These areas and flood conditions included debris washed into Claytor Lake, and water inundation height in the town of Damascus, Virginia. Regarding Claytor Lake, a rule has been historically applied that debris detected in the water can be assumed to be one foot thick, and by knowing the acreage of floating debris, the cubic yards of debris removal can be estimated [1]. In our work, we show that these estimates are not accurate. Likewise, obtaining water inundation heights in structures requires ground-based measurements at every building, which is a prohibitively time-consuming activity and can only be completed once a crew is available for the work. Our work presents a water height analysis based solely on aerial imagery, which is easy to obtain if the area is unreachable by a trained crew.

For household debris, FEMA uses the debris estimation guide [18] and multiplicative factors to estimate the debris from residential and/or commercial structures. In the case of single-family residential houses, FEMA developed a formula for debris estimation based on the empirical study:

$$CY = SF \times 0.2 \times VCM \quad (1)$$

Here, CY is the cubic yards of debris, SF is the building square footage, 0.2 is a constant based on the study, and VCM is a vegetative cover multiplier (ranging from 1.1 to 1.5 depending on neighborhood canopy maturity). To find the CY for the whole town, an average SF is taken and then multiplied by the number of houses.

According to the Robert T. Stafford Disaster Relief and Emergency Assistance Act [24], a preliminary damage assessment (PDA) is performed by FEMA to evaluate the extent of damage caused by a disaster [18]. FEMA conducts windshield surveys as (PDA) in which the personnel go door to door, interview residents, and take photographs to classify the damage to structures as Affected, Minor, Major, or Destroyed [25]. According to FEMA and associated documentation, this classification is based on observed damage levels, including factors like water depth, contamination, and foundation integrity. Damage-percentage thresholds are commonly used: Affected for cosmetic or non-structural damage, Minor for less than 25% structural damage, Major for 25–50%, and Destroyed for greater than 50% [26]. These percentages are multiplied by the CY calculated in Equation (1) to estimate the total debris from each house. This method is inherently time-consuming, labor intensive, and often delayed due to access issues, safety concerns, or large-scale damage. The subjective nature of field assessments can also introduce inconsistency. These delays ultimately affect how quickly communities receive funding for cleanup and repairs. With the integration of flood modeling and geospatial tools, the flood impact on the buildings and classification of damage can be performed prior to field visits. Using analysis products developed by the NOAA National Water Prediction Service that include Flood Inundation Mapping (FIM) [27], and the NOAA National Severe Storms Laboratory (NSSL) Flooded Locations and Simulated Hydrographs (FLASH) [28], a future nationwide project predicting property loss is realizable. This would serve communities in the early-warning phase as well as FEMA, insurance companies, USACE, and local governments during the post-disaster response and recovery phase.

Further, this debris estimation is multiplied by the cost of cleanup per CY to estimate the debris cleanup cost. These general methods are useful for debris management planning, but they do not factor in property value. That analysis is available using a Hazus analysis [29] which was developed by FEMA. Because the Hazus code is not well supported, it does not find popular use in disasters today, so the property value aspect does not factor into a recovery analysis. Combining a hydrology model with property information can give a much more accurate picture of damage and help in determining if a structure qualifies for the federal disaster declaration.

We have provided those tools in this paper and demonstrated how it works in the Damascus community, showing significant time savings to determine whether or not the damage qualifies a community for a federal disaster declaration. We have studied a few houses in Damascus and based on the water height estimated using HEC-RAS and the property information on GIS—such as property type and value, and number of stories—evaluated the loss of the property. Having an accurate estimate of the damage caused will help FEMA in planning the fund relief for the community.

Higher definition debris estimation in streams is also demonstrated using the same low-cost, single-camera aerial imaging payload mounted to the motorglider. The presented work shows the ability to rapidly estimate debris deposits in waterways using aerial imagery which reduces the time and cost of recovery by potentially several months. The use of photogrammetry to obtain these estimates is limited to cases where there is an unobstructed view of the ground terrain, i.e., tree canopies do not obscure the view. The solution in these cases would be to use a scanning LiDAR system which does not have the same limitations as visual imagery-derived 3D reconstructions; however, the payload would be considerably more expensive.

Aerial imagery was captured using a GoPro Hero 9, 20 MP camera (GoPro, Inc., Guadalajara, Mexico) mounted on the wing of a Phoenix U-15 Motorglider, overcoming the challenges of using UAVs to cover vast areas. The GoPro is a very simple and cheap solution to collect imagery to build 3D reconstructions and orthomosaics of the environment and a notable contribution for the disaster response community which is more likely to use aircraft equipped with expensive payloads. Advances in structure from motion (SfM) based softwares allow usable reconstructions with these DIY systems.

The SfM-based OpenDroneMap [30] was used for reconstruction and orthomosaic creation from the imagery. For lake debris estimation, we used Roboflow [31] to manually segment the images using the smart polygon tool. After segmentation, we applied the Canny edge detection method on the original image of the extracted lake and color thresholding in HSV colorspace, giving the final segmentation of debris. The debris was then quantified in acres by analyzing pixels corresponding to edges and thresholded regions. For land and stream debris estimation, we used the pre-disaster 2016 state LiDAR DEM data and compared it with the DEM data from 3D reconstruction to estimate the height of debris in different regions of Damascus. We further performed the flood modeling in HEC-RAS to estimate the flood water depth in the town which can be used by FEMA to estimate the damage using a Hazus based tool.

The rest of the paper is organized as follows: Section 2 includes the workflow of various tasks and the corresponding time required to perform debris estimation. It also explains in detail the various methods and software employed in the process. Section 3 shows the results of the analysis of lakes and towns and their comparison with the debris collected in the field. Finally, conclusions and future work are provided in Section 4.

2. Methodology

2.1. Flow Chart of Data Management

The general workflow for the debris estimation is shown in Table 2 and Figure 1. In the first step, data is collected with an aircraft equipped with a nadir-oriented camera. The next step is 3D reconstruction using the geotagged images processed using any structure-from-motion software which is OpenDroneMap for this project. This step gives us an orthomosaic image and a raster DEM which can be analyzed in ArcGIS. ArcGIS is used in two different ways for estimating debris in the lake and on land. For estimating lake debris, ArcGIS is used to roughly select the lake area and divide it into small regions or patches. This was performed to enable segmentation of the lake class from the whole image using Roboflow [31].

Table 2. Resource allocation to each task .

Task	Resources
Aerial imagery collection	Airplane, certified pilot
3D reconstruction and orthomosaic image	Geotagged images, ODM version 3.5.4
Division of lake into segments	ArcGIS Pro 3.3.2
Debris segmentation and classification	Roboflow (online cloud-based)
Estimation of debris on land	ArcGIS Pro version 3.3.2
Flood water depth estimation	HEC-RAS version 6.6

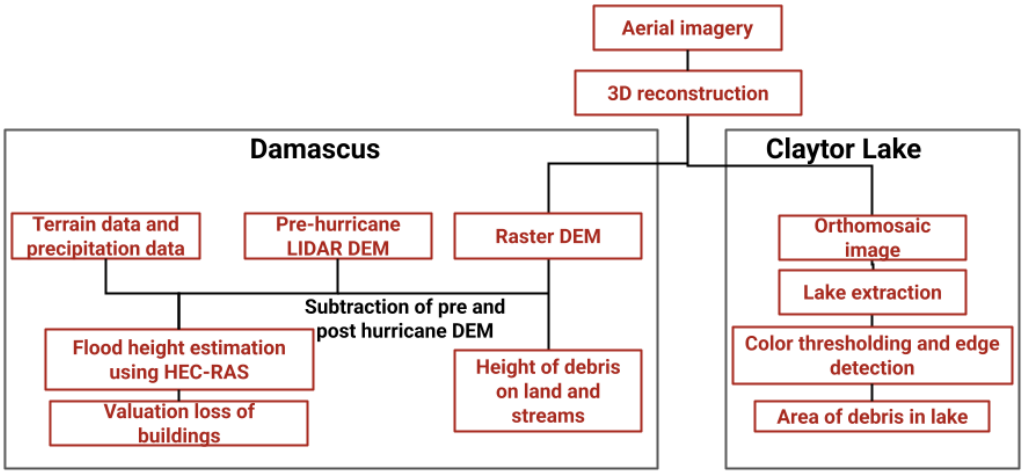

Figure 1. General workflow for debris estimation.

For estimating the height of debris on land, we first visually select the areas where there is debris using ArcGIS and then for each of these areas, compute the difference between the 2016 LiDAR data and raster DEM data. We also perform flood modeling in HEC-RAS to estimate the flood depth. These flood heights are then used to evaluate the damage caused in commercial and residential buildings using a Hazus-based tool.

2.2. Aerial Imagery—Study Area and Data Collection

The areas to be surveyed, Claytor Lake and Damascus (Figure 2), were overflown using a crewed aircraft: the Phoenix U-15 Motorglider equipped with a GoPro Hero 9 camera payload mounted to the wing of the airplane in a nadir orientation (Figure 3). Set up to capture 20 MP images, the camera took pictures every two seconds resulting in image overlap of nominally 82% for a speed of 50–60 kts at an altitude between 700 and 2000 ft AGL. The ground resolution was nominally 15 cm. A flight plan was generated for all areas

using ForeFlight as shown in Figure 4 to create line spacings (pitch) that also resulted in sufficient overlap for 3D reconstruction.

Figure 2. Study area: Claytor Lake in red marker and Damascus in blue marker.

Figure 3. Phoenix U-15 Motorglider (Photo courtesy of Jeff Shingleton).

Flights were staged at Virginia Tech/Montgomery Executive Airport (KBCB). The Phoenix has an endurance of about six hours, allowing flights to originate from KBCB and reach all areas of interest with sufficient endurance to complete the imaging profiles. The Claytor Lake flight covered 1600 acres of lake area observed to contain debris, with a serpentine flight path chosen in order to cover the main lake area but also inlets that showed debris evidence (Figure 4a). After this flight, the imagery was collected over South Holston Lake, covering a shorter section of around 285 acres, which was also affected by the hurricane. South Holston Lake imagery will be used to evaluate our methodology and validate its metrics. The aircraft then flew to Damascus (Figure 4b) to further collect imagery in the town. Upon completion of this data collection, additional areas of interest were overflown before the aircraft returned to Blacksburg 3 h and 4 min later.

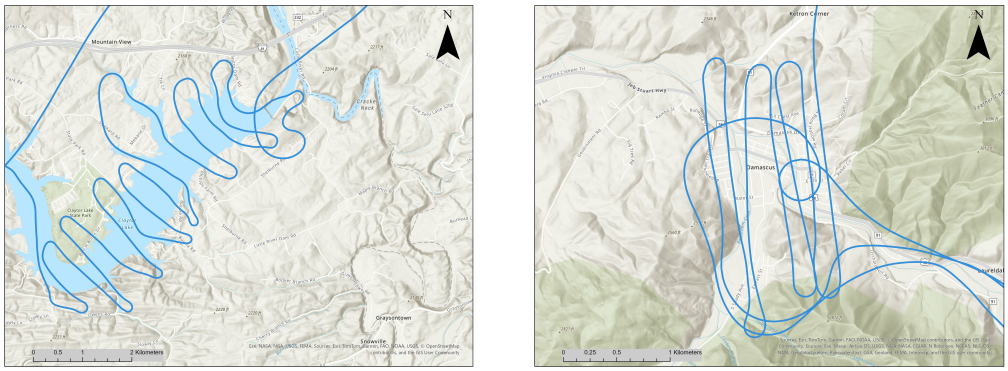

(**a**) (**b**)

Figure 4. Flight path in (**a**) Claytor Lake and (**b**) Damascus using ForeFlight, KML plotted on ArcGIS Pro.

2.3. Three-Dimensional Reconstruction

Three-dimensional reconstruction is created using a sequence of images by capturing the geometry and appearance of objects in three dimensions. While 2D imagery provides a limited amount of information, converting the 2D images into a 3D model amplifies the information. The 3D reconstruction is invaluable for analyzing spatial relationships, such as assessing elevation differences between objects.

There are various methods to perform 3D reconstruction using different sensors. Sensors such as LiDAR and laser scanners provide precise measurements but are often expensive and require specialized equipment. Alternatively, reconstruction using RGB images is a cost-effective and accessible solution, particularly when leveraging techniques like SfM.

2.3.1. Structure from Motion (SfM) Using OpenDroneMap

SfM [32–34] is a widely used pipeline for 3D reconstruction that utilizes standard RGB images captured from different camera views and locations. This method generates a 3D map in the form of a sparse point cloud and also estimates the positions and orientations of the cameras. Broadly, it has two stages. In the first stage, it focuses on finding a relationship between images by detecting and matching local features, such as corners and edges. These features are essential for understanding the structure of the scene. After extracting features, it compares them across images and ensures alignment between images with overlapping fields of view. In the next step it checks false correspondences using geometric constraints like the epipolar geometry. The result is a scene graph, where each node represents an image, and edges denote geometrically verified image pairs.

In the second stage, SfM iteratively reconstructs the 3D scene by estimating camera poses and generating a sparse point cloud. It registers two images with sufficient overlap, estimates the relative orientation of this pair, and generates the first set of 3D points. With the initial camera poses, it performs triangulation to generate more 3D points. As more images are added, the initial estimates of camera poses and 3D points are refined through bundle adjustment that minimizes the reprojection error, and ensures accuracy of the reconstruction.

The result of this process is a sparse 3D point cloud, capturing the structure of the scene. In this paper, we utilize ODM [30] software which is based on SfM to perform 3D reconstruction. ODM is an open-source toolkit that converts 2D images into a 3D point cloud and generates Georeferenced Orthorectified Imagery and DEM [35]. An example of a portion of the 3D Textured Model created for Damascus is shown in Figure 5.

Figure 5. A portion of the 3D textured model of Damascus created using OpenDroneMap.

2.3.2. Definitions

DEMs represent the Earth's surface in three dimensions, capturing variations in terrain elevation. These models are especially useful for applications like flood modeling and urban planning. A DEM is typically represented as a raster grid, where each cell holds the elevation value for a specific geographic area. It provides essential information for understanding the topographic features of the terrain.

Orthorectified images are georeferenced images that have been geometrically corrected to eliminate distortions caused by camera tilt and terrain relief. Orthoimages serve as a base layer for Geographic Information Systems (GISs) [36].

Figure 6 shows an orthorectified image of a portion of Damascus that was generated using ODM.

The 3D point cloud, orthorectified imagery, and DEM become the input of the debris analysis in Claytor lake and Damascus.

2.4. Debris Estimation in Claytor Lake

Computer vision is a powerful tool for analyzing image data and extracting information from it. In this study, we incorporate methods like edge detection and color thresholding to estimate the amount of debris in the lakes. However, to extract accurate information using these approaches, we need to separate the lake and the land regions using segmentation techniques.

2.4.1. Segmentation

To avoid the time and resource burden of training custom models, some pre-trained machine learning tools—such as Mask R-CNN [37] and Segment Anything Model (SAM) [38]—have been explored. Mask R-CNN is a popular model for instance segmentation; however, it is trained on the MS COCO dataset [39], which includes 80 object categories such as people, vehicles, furniture, and buildings. However, it lacks specific classes for land, water, or debris, making it unsuitable for environmental segmentation tasks without significant fine-tuning. On the other hand, SAM is trained on a much larger and more diverse dataset, enabling it to adapt to a wide range of segmentation tasks. SAM also offers a browser-based demo [40] that allows users to upload an image and generate segmentation masks interactively. We apply SAM to our own aerial images (Figure 7) to

assess its performance. While it shows potential, the tool fails to detect several land regions, highlighting its limitations for delineating land and water with debris.

Figure 6. Orthorectified image of Damascus.

To extract the lake region from the images, we employ Roboflow. Roboflow [31] is an online cloud-based platform that allows for labeling, annotating, and augmenting datasets. It features an AI-assisted Smart Polygon tool [41] that can be used to create a polygon around the object of interest in the image. This tool uses machine learning algorithms to suggest shapes for any object that we click on. However, Roboflow has a restriction that it can only process an image that is less than 20 MB in size. Due to the large size of the orthomosaic images generated from ODM, which often exceed GBs, we use ArcGIS to divide the lake into smaller, non-overlapping, manageable sections (see Figure 8). The lake boundary shapefile is split into smaller sections, after which a Python script in the ArcGIS Python (version 3.11) Notebook is used to automate the masking process, generating image chunks under 20 MB in size. These sections are then uploaded to Roboflow for segmentation.

Figure 9a shows one section of the Claytor Lake, and Figure 9b illustrates the segmentation for that section in Roboflow. The resulting masks separate land from water, enabling us to isolate the lake regions. The corresponding lake area without land after applying the mask is shown in Figure 9c.

Once the lake regions are segmented, we employ two complementary methods for detecting debris within the water.

2.4.2. Color Thresholding

We use HSV colorspace (hue, saturation, and value) for color thresholding. HSV colorspace is a way to represent colors where hue defines the type of color, saturation indicates the intensity, and value represents brightness. This method detects all the objects falling in the HSV threshold range selected. Debris, primarily composed of wood, plastic,

mulch, and mud, is identified based on its color properties. Using the HSV colorspace, we detect debris with hue values between 120 and 149. The range of saturation and brightness is kept as 0 to 255. Variation in lighting and environmental conditions may require adjustments in the HSV threshold range for different image sets.

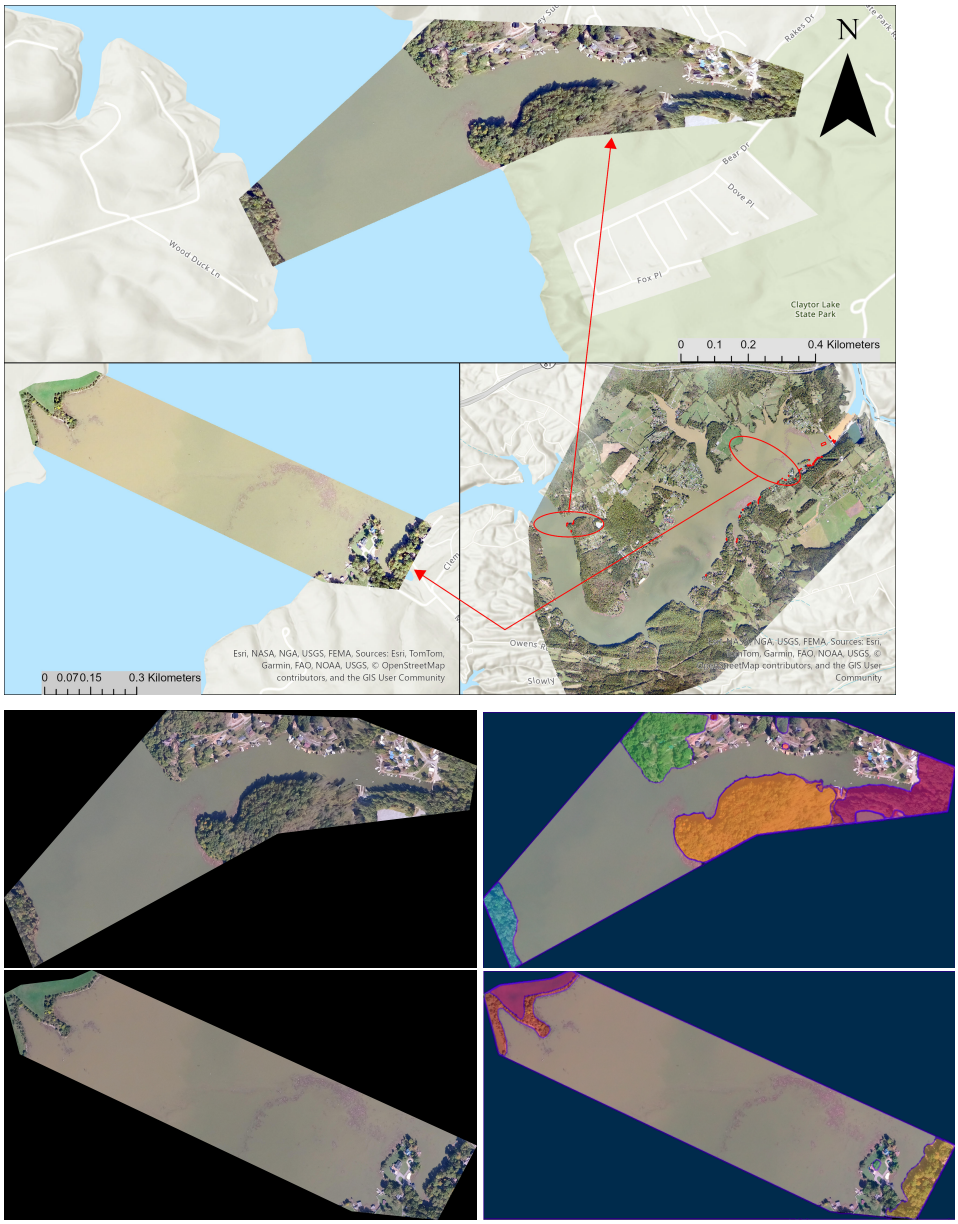

(**a**) Section of the lake (**b**) Section segmented using SAM

Figure 7. Segmentation of sections of Claytor Lake using SAM, showing that SAM is not able to segment the entire image. The top panel shows the inset map of the lake with highlighted sections analyzed below. The bottom panels show the original aerial images and their corresponding SAM segmentations.

2.4.3. Edge Detection

While color thresholding is useful in detecting debris in the HSV range, it faces limitations when dealing with variations in lighting and depth. For example, color thresholding alone cannot reliably differentiate debris based on thickness, such as mulch, which appears to be 2–3 inches deep, versus logs that can be 6–12 inches deep as shown in Figure 10.

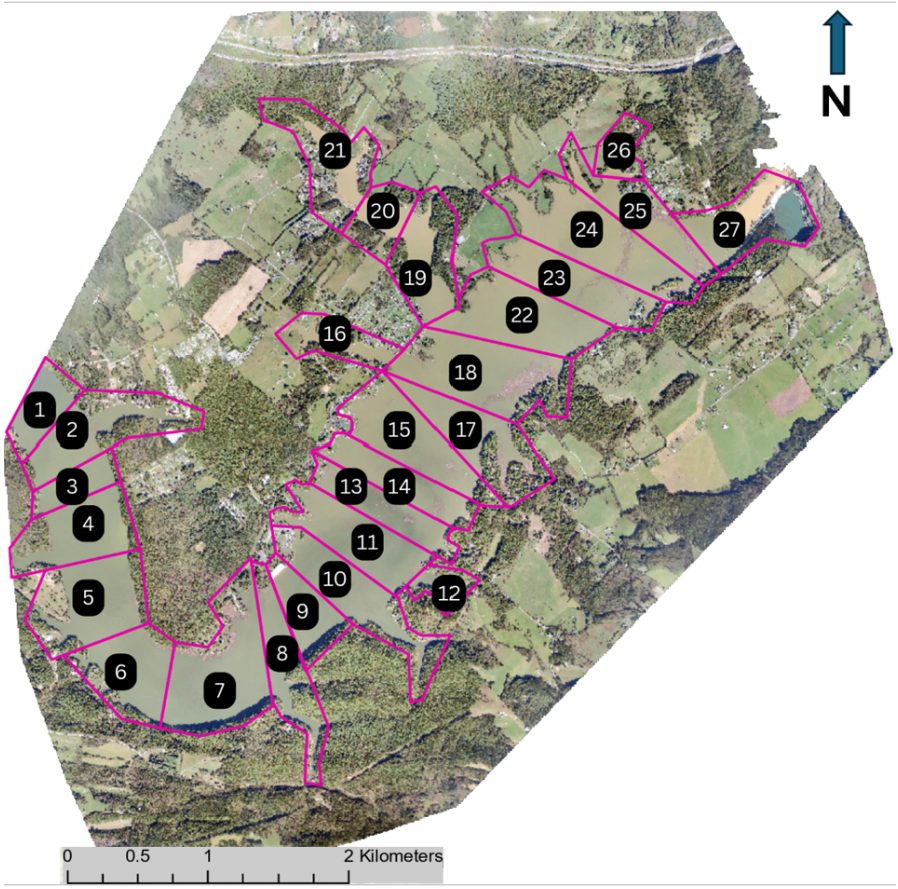

Figure 8. Orthomosaic image of Claytor Lake with 27 sections as pink polygons. Each section is labeled for reference in subsequent figures.

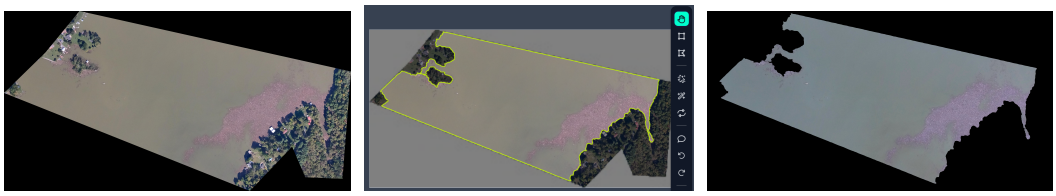

(**a**) Original section (**b**) Segmentation in Roboflow. (**c**) Extracted lake

Figure 9. Segmentation of section 18 from Figure 8 of Claytor Lake in Roboflow (figures not to scale and orientation).

To improve debris detection and capture the difference between log and mulch, we apply Canny edge detection. The Canny algorithm is applied to contrast-enhanced grayscale images using threshold values of 50 and 150. To account for the physical thickness of logs visible in aerial imagery, we dilate the edges using a square kernel of size 4 × 4 pixels, which approximates half the average log width based on visual inspection. This step ensures a conservative overestimation of debris where necessary. However, edge detection also detects the boundary of the lake as an edge. To avoid misclassifying the lake's boundary as debris, we subtract edge pixels corresponding to the lake boundary from the total edge detected pixels.

The results, shown in Figure 11, illustrate the detection process. Edge detection highlights the potential debris boundaries in green (Figure 11b). Color thresholding identifies debris based on specific hues, represented by blue pixels (Figure 11c).

The results from color thresholding (blue pixels) and edge detection (green pixels) generate overlapping and distinct pixels, and thus we combine both results and create two classes as shown in Figure 12. Class 1 (red pixels) represents the overlapping debris

detected by both edge detection and thresholding, while Class 2 (yellow pixels) shows the debris detected by either edge detection or thresholding. The summation of debris from both classes represents the total area of the lake covered with debris. Since big logs and other materials are typically lying densely with the mulch, these objects are detected as overlapping debris or Class 1. Consequently, Class 2 would represent the non-overlapping debris which also includes the debris that is scattered sparsely and can include some logs away from the dense debris as shown in Figure 13.

Figure 10. Claytor Lake debris images. (Photo courtesy of Virginia Department of Emergency Management).

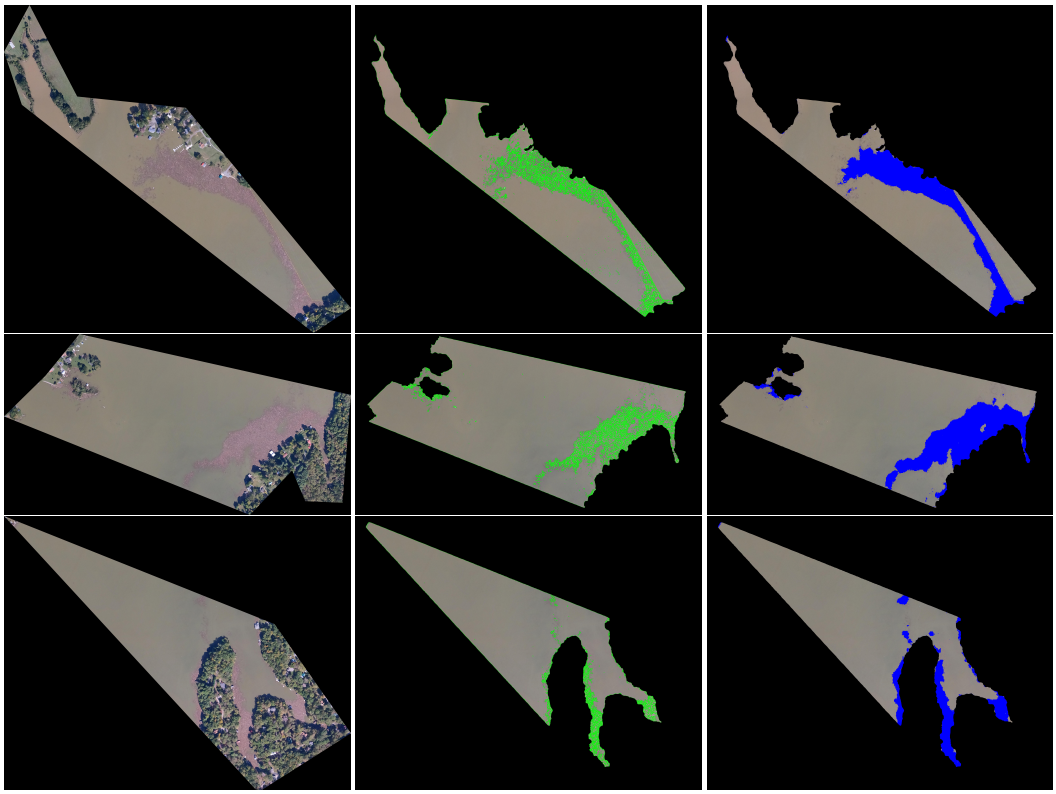

(**a**) Sections of the lake (**b**) Edge Detection (in green) (**c**) Color thresholding (in blue)

Figure 11. Debris detection results for Claytor Lake. Each row corresponds to a section (17, 18, and 25 from Figure 8), showing the original image, edge detection, and debris thresholding. (Figures not to scale and orientation).

2.5. Debris Estimation in Damascus

Damascus was heavily flooded after Hurricane Helene, resulting in debris deposits throughout the town. We can compare the debris and resulting damage by visually comparing the ODM image with pre-hurricane satellite imagery from Google Earth as

shown in Figure 14. While the visual comparison clearly indicates extensive debris deposits, a quantitative estimate is necessary to assess debris volume and distribution. This requires a comparison of pre- and post-flood elevation models, described in the following sections.

2.5.1. Debris Estimation on Land

For debris estimation in Damascus, we compare the pre-flood 2016 LiDAR-derived DEM with the post-flood DEM generated from ODM to estimate debris height. The comparison is performed in ArcGIS Pro 3.3.2.

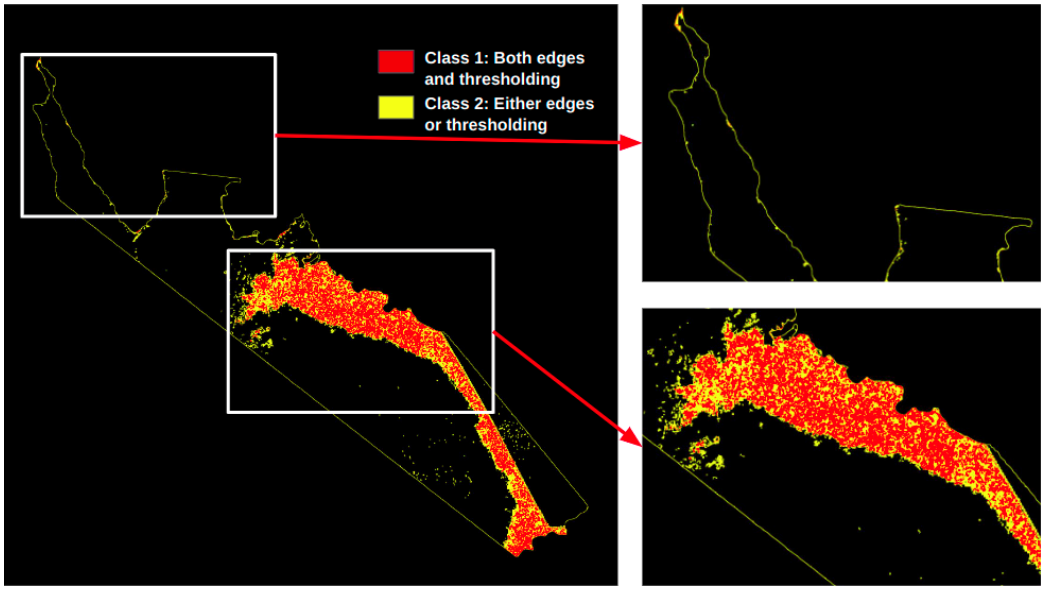

Figure 12. Classification of debris into two classes on section 25 from Figure 8 (Figures not to scale and orientation).

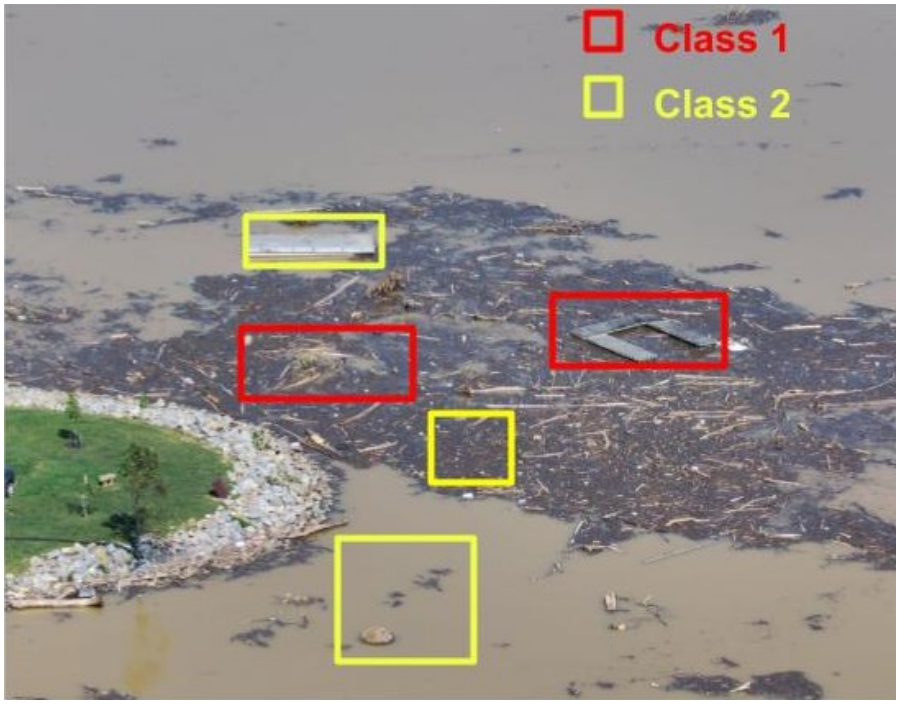

Figure 13. Debris marked with Classes: Class 1 represents the objects lying in dense debris, while Class 2 represents the mulch and scattered debris (Figure not to scale) (Photo courtesy of Virginia Department of Emergency Management).

Figure 14. A comparison of pre-hurricane satellite images (**left column**) with post-hurricane ODM orthophotos (**right column**) at three locations (Sections 3, 11, and 10 (top to bottom) from Figure 15) in Damascus. The images on the left are presented at a similar scale to those on the right.

Pre-flood LiDAR point cloud data is obtained from the Virginia Geographic Information Network (VGIN). Since the DEM for the Damascus section was corrupted on the site, the point cloud data is processed in ArcGIS Pro to produce a DEM at 1 m resolution. The UAV-derived DEM from ODM has a spatial resolution of 8 cm and is resampled to 1 m to ensure a uniform basis for comparison. The coordinate systems are also aligned: the LiDAR DEM (originally in NAD 1983 (2011) UTM Zone 17N) is reprojected to WGS 1984 UTM Zone 17N to match the ODM DEM.

When comparing DEMs, we find a varying vertical offset of 33–35 m across the study area, making a single correction value impractical. To address this, Damascus is divided into several debris segments as shown in Figure 15. In each segment, leveled ground points such as roads and open grass areas, with no debris, are used to determine the average offset. This offset is then applied to correct the ODM DEM for that specific segment.

After correction, we use the Raster Calculator to adjust the segmented ODM DEM and then perform raster subtraction against the LiDAR DEM to determine debris heights. Some discrepancies remain due to outliers such as trees and buildings since LiDAR and ODM pixel alignments do not perfectly match. To minimize the influence of these outliers, we calculate the median pixel height within each segment using Zonal Statistics in ArcGIS Pro. Finally, the median height of the debris for each segment is multiplied by its debris-covered area to estimate the volume of the debris.

Figure 15. Sections of Damascus with debris highlighted with red boundaries. Each section is labeled for reference in subsequent figures.

2.5.2. Debris Estimation Around Streams and Open Spaces

The impact of the hurricane extends beyond residential areas and infrastructure, significantly affecting nearby streams. Figure 16 shows the stream section in Damascus that is studied.

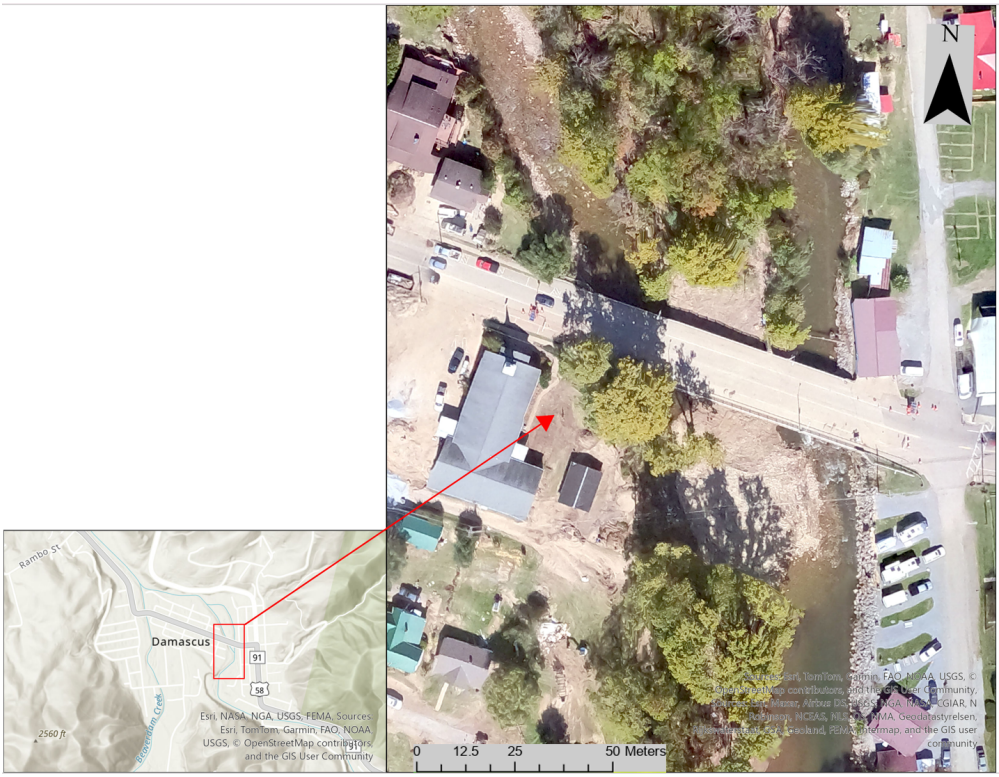

Figure 16. Section close to the stream in Damascus with debris and erosion, analyzed for volume computation.

Although the approach in Section 2.5.1 is effective for built-up and tree-covered areas, stream corridors present additional challenges. These areas are affected by both deposition and erosion, and LiDAR data is often incomplete over water bodies. Therefore,

a modified method is used for streams and adjacent open spaces. After adjusting the offsets, raster subtraction is performed to calculate the height difference within the pixels. Instead of taking the median height, which is performed in Section 2.5.1, each pixel's actual height difference is used to calculate the volume. This can be done because this stream section/open space does not have any misaligned buildings, cars, or tree canopies that affect the height calculation. The volume of eroded and deposited pixels is calculated based on the raster values in ArcGIS Pro.

2.5.3. Flood Modeling in Damascus

In order to model the water depth in Damascus during the flood, HEC-RAS is used to perform simulations. HEC-RAS is an open-source software that is used to perform one- and two-dimensional flow calculations, sediment transport, and mobile bed computations [42].

The terrain data for the simulation is obtained from the Virginia LiDAR database [43] as a one-meter resolution DEM from 2016. This DEM is used for flood modeling in Damascus as shown in Figure 17. During a visit to the area and consultation with local authorities, we confirmed that the build-up in front of the bridge shown in Figure 16 is caused by deposition during the flood. It was also noted from eye-witness reports that flood water is diverted at the bridge into town because of this chokepoint. Since the HEC-RAS simulations do not use sediment flow (due to time constraints), this location of the stream is adjusted to accurately represent the inability of water to flow through the stream at this location.

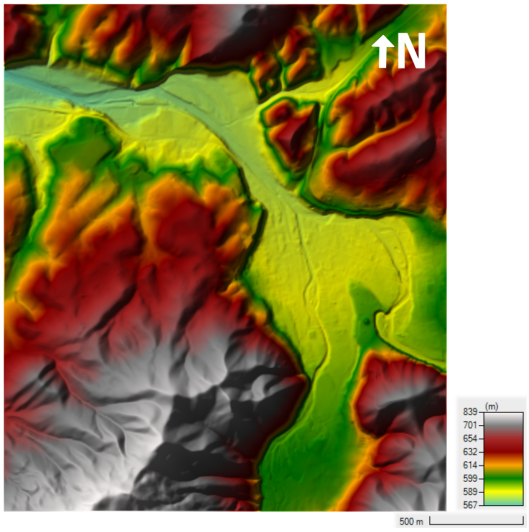

Figure 17. The DEM of the Damascus watershed, used for the flood simulations performed in HEC-RAS.

The land cover data for our simulation is acquired from the 2021 National Land Cover Database (NLCD) [44]. In HEC-RAS, this land cover data requires corresponding Manning's N values and percent impervious values. The Manning's N value is a roughness coefficient specific to a land cover class and varies depending on the geographic location of interest. As a result, the Manning's N value requires careful selection on a case-by-case basis and cannot blindly be applied to land covers. As a starting point, however, the Manning's N values and percent impervious values for the land cover classes are set based upon recommended values from HEC-RAS documentation [45].

Using the recommended Manning's N values, the exact Manning's N values for the land cover in our HEC-RAS simulation are derived from the dissertation of Whitehurst [46]. His research focused on the modeling of flooding events in Hurley and Eastern Kentucky and generalized the methodology to the broader Appalachian region. In the case of Kentucky, flood simulations were validated using observed streamflow and gauge

height data from two USGS monitoring stations. The use of official USGS gauge data provides confidence in the reliability of the model calibration and Manning's n values reported in the study. Since Damascus is located within the Appalachian region and shares similar topographic and hydrologic characteristics, we adopt the same parameterization approach. The final land cover classifications and their associated Manning's n values used in our model are the same as the base values recommended in [45], except for values for Shrub-Scrub, Woody Wetlands, and Emergence Herbaceous Wetlands set as 0.08, 0.08, and 0.06, respectively.

The HEC-RAS simulation is performed using two-dimensional unsteady flow simulations. For our test area, 10 m by 10 m spacing is used to create the flow area mesh. In addition to this, breaklines are enforced along the length of the stream to better refine the mesh along the stream. The unsteady flow analysis is performed using a computation interval of two minutes with a time step adjustment allowed to ensure a maximum Courant value of one for the simulation. This threshold is set to ensure the stability of the computation. The inlet boundary condition is set as a flow hydrograph. Additionally, uniform precipitation is used since the area is small enough to allow this uniform assumption. The flow hydrograph and precipitation values are acquired from the National Oceanic and Atmospheric Administration, Multi-Radar Multi-Sensor (NOAA MRMS) System [47]. Q3 Multi-Sensor precipitation is used with a one-hour time interval, and CREST flow is used to estimate the inlet flow for the simulation area. The MRMS CREST flow is used due to the lack of streamflow gauges in this area. The HEC-RAS unsteady flow simulation is performed between 25 September at midnight and 28 September at 11 pm.

2.5.4. Damage Analysis of Buildings

The flood water height can be estimated at any location using HEC-RAS modeling and can be used by agencies like FEMA in planning the fund relief for the community. Estimating valuation loss due to flooding in the town of Damascus involves utilizing the depth–damage curves based on Hazus flood analysis, which relates the floodwater height in buildings to the corresponding damage ratio. With the floodwater height obtained in six sample buildings as shown in Figure 18 from HEC-RAS, we estimate the valuation loss for those structures.

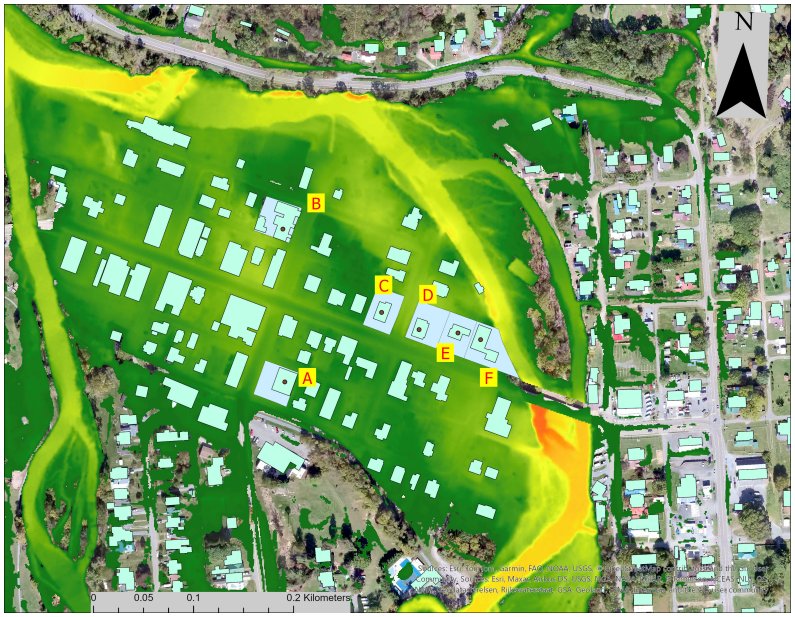

Figure 18. Sample buildings A through F, chosen for valuation loss calculation in Central Damascus.

Information related to the buildings and valuations in Damascus is downloaded from Washington County Geospatial Web Portal [48], which was recently updated in January 2025. We select a few buildings, including commercial properties and residential houses, to extract key information such as building types, valuations, story counts, and locations. Since the shapefile's building type descriptions are different from the FEMA categories [49], we need to re-classify the buildings based on the number of stories and assume all buildings have a basement (to be on the conservative side, this assumption is made, as basement details are not available in the shapefile). This GIS-based data is integrated with floodwater depths derived from the HEC-RAS model along with the FEMA building categories.

The depth–damage curves shown in Figure 19 developed by NHERI SimCenter [50] are then used to find the damage ratio for each building based on the floodwater height. The valuation loss of each building due to flooding can be estimated by multiplying the damage ratio with the property valuation.

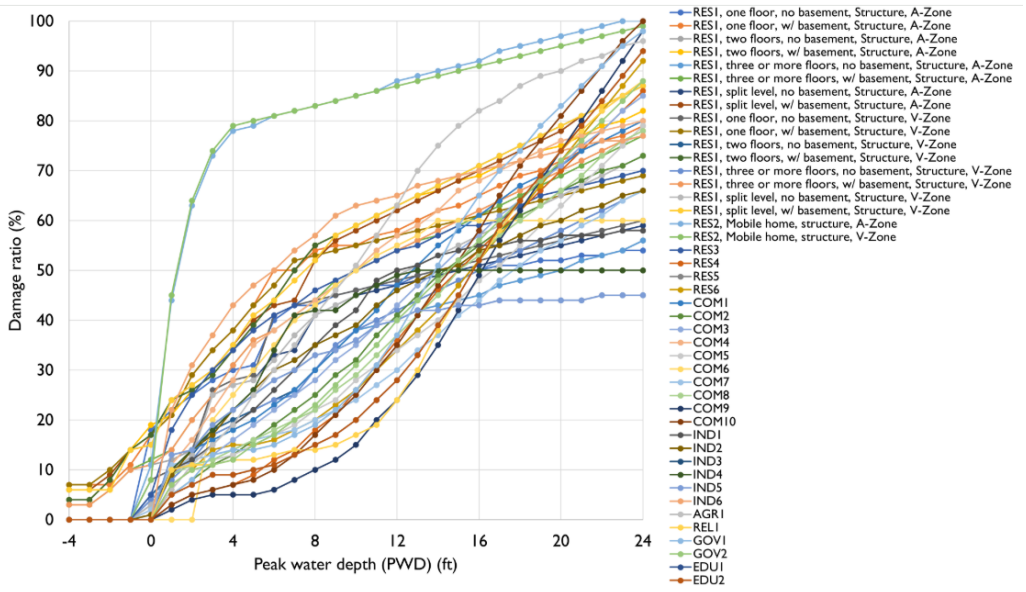

Figure 19. Depth–damage curve. Reprinted/adapted from the NSF NHERI SimCenter R2D Documentation [50], licensed under the BSD 2-Clause License (Copyright The Regents of the University of California).

3. Results and Discussion

This section discusses the results for Claytor Lake and Damascus debris estimation, flood modeling, and property valuation.

3.1. Debris Estimation in Claytor Lake

In Section 2.4, we present the implementation of a pipeline of two segmentation approaches that proved effective, allowing for accurate lake isolation and subsequent debris detection. To estimate the total debris in the lake, we calculate the percentage of debris pixels relative to water pixels for each section of Claytor Lake. The area of the lake is determined to be around 1552 acres based on pixel analysis. Our model estimates approximately 90 acres of debris.

We compare our findings to data provided by DEQ, which reported 28,249 cubic yards of debris, which is 17.5 acre-feet. USACE assumes 12 inches of debris, and based on that assumption, the debris is spread over an area of 17.5 acres. However, there is no basis for the one-foot assumption, as it cannot represent the debris of varying depth.

As explained in Section 2, we classify the lake debris into two classes, with Class 1 representing mainly the logs and plastic, and Class 2, the mulch. This classification can

be used to find the volume of the debris. For conservative estimates, we can assume that class 1 contains only logs that have the highest thickness of all debris detected. Based on this assumption, the volume of debris is estimated as shown in Table 3.

Table 3. Debris volume estimation in Claytor Lake.

Class	Area (acres)	Depth (in)	Volume (acre–ft)
Class 1	33	6–12	16.5–33
Class 2	56.4	2–3	9.4–14.1
Total	89.4		25.9–47.1

This table shows that class 1 debris can have a volume from 16.5 to 33 acre–ft, and class 2 debris can be 9.4 to 14 acre–ft, reflecting a possible variation in debris spread and thickness. Another possible scenario is that the debris collected by USACE is mostly represented by class 1, which is 33 acres. With a depth of 6.5 inches, the debris of 33 acres is estimated to be around 17.5 acre–ft, which is the same as the collected debris.

There are several factors contributing to the potential errors in our method. Edge detection, being a sensitive process, sometimes misclassifies ripples and sunlight reflections on the lake surface as debris, contributing to the false positives as shown in Figure 20a,b. In our case, this accounts for 3.4% of the total debris and is found in 3 out of 27 sections. Throughout the process, we approximate the edge thickness to half the average log width, but the actual log sizes can vary. By changing the edge width from 4 pixels to 2 pixels, the debris is reduced by around 14%. Additionally, during segmentation in Roboflow, small debris patches near the lake boundary are occasionally excluded. Moreover, certain areas, such as boats or floating platforms, are difficult to distinguish from debris and thus are not excluded from the debris estimation. Further, some areas are obscured by shadows where the algorithm fails to detect visible debris, resulting in false negatives as shown in Figure 20c. It is also important to note that the DEQ data is collected nearly two months post-flood. By that time, some debris, particularly wood, may have sunk to the lake bottom, reducing visible debris quantities.

To evaluate the applicability and validity of our segmentation method, we implement the methodology on aerial imagery collected from the mapped South Holston Lake area, which is processed similarly to Claytor Lake. The orthomosaic is divided into 50 sections and analyzed for debris assessment. Based on our analysis, we estimate approximately 12 acres of debris present within the lake. All parameters for edge detection and color thresholding are kept consistent across the sections, except for one instance, where the hue threshold range is expanded from 120–149 to 110–149 to accommodate color variation. The false positives, primarily due to the misclassification of sunlight reflection as debris, are 0.19% of the total lake area, occurring in 4 out of 50 sections. False negatives, where debris is obscured by shadow and is not detected, represent approximately 0.44% of the total water area.

Table 4 represents the confusion matrix and evaluation metrics of the edge detection and color thresholding-based segmentation method for Claytor Lake and South Holston Lake. The false positives, false negatives, true positives, and true negatives are calculated as percentages of the total water, including debris.

Despite these challenges, our method provides better initial estimates as compared to the USACE estimates and can be obtained within 72 h after the disaster. The sectional division of the whole mapped Claytor lake area of nearly 2400 acres on ArcGIS Pro takes approximately 1–2 h on a machine with 12 GB RAM and i5, 10th-gen processor, while segmentation in Roboflow takes nearly half an hour for 27 sections. This step highly depends on the number of sections created. Since Roboflow is an online platform, it does

not depend on the hardware in use. These segmented images can then be fed to the algorithm of color thresholding and edge detection to detect the logs and discoloration in the lake. This algorithm is run on an i7 12th-gen machine with 24 GB RAM and can produce the result in less than a minute for nearly 27 sections of the lake.

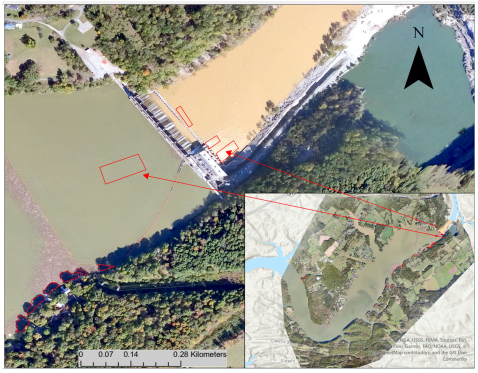

(**a**) Example of sunshine on water misclassified as debris (false positive)

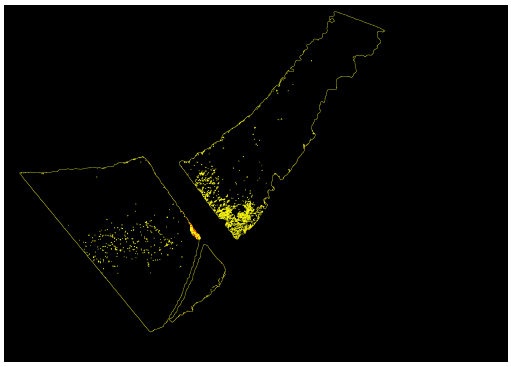

(**b**) Sunshine misclassified as debris (yellow, false positive)

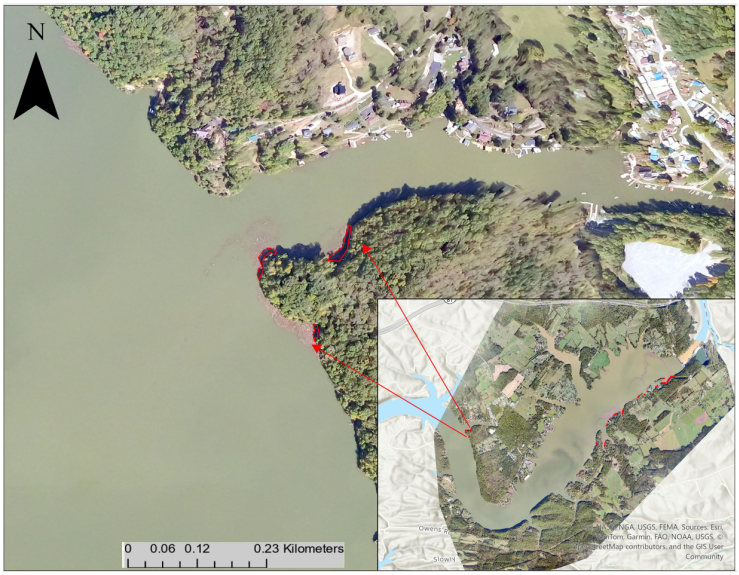

(**c**) Example of shadow containing debris (false negative)

Figure 20. Sections of Claytor Lake with false positives and false negatives: (**a**,**b**) false positives due to sunshine, (**c**) false negative due to shadow containing debris. (Approximate location for both cases shown in red polygon).

Table 4. Confusion matrix and evaluation metrics of the edge detection and color thresholding-based segmentation method.

	Actual: Debris (%)	**Actual: Water (%)**	**Metrics (%)**
Predicted: Debris	4.8	0.2	Precision: 96.9
Predicted: Water	0.3	95.0	Recall: 94.1
			Accuracy: 99.5

Our current study focuses on lakes devoid of large objects like tires or propane tanks. For lakes with such objects, object detection algorithms can be incorporated to exclude docks, boats, or other non-debris objects from analysis. Adjusting the thresholding range and edge thickness can further refine debris detection in complex scenarios.

3.2. Debris Estimation in Damascus

The proposed method of comparing pre-flood LiDAR and post-flood ODM DEMs allows the estimation of debris deposition and erosion on land and around streams. This process takes nearly 5–6 h on a machine with 12 GB RAM and i5, 10th-gen processor for a 2 square km area. Figure 21 shows the debris map of a section in Damascus. The calculations estimate the debris of 10,950 cubic meters in the town. The height of debris observed is in the range of 0.16–0.61 m, with high standard deviation values. It suggests that our data is not ideal for such fine-scale calculation. Moreover, we do not have any ground truth to validate our data.

Figure 21. Debris map of sections 3 and 4 of Figure 15 of Damascus. Here, blue represents erosion, red represents high debris, and green and yellow represent moderate debris deposits. (For visual purposes, height differences beyond +2 m and −2 m are omitted for this map, as they are mostly outliers due to misaligned tree and structure heights and shadows).

For debris estimation around streams, we separate the difference raster into two distinct rasters for better visualization and perform volume calculations for erosion and deposition areas separately. The raster is classified as "eroded" if the height difference is negative, and as "deposits" if the height difference is positive.

In Figure 22, we can observe the section around the stream with erosion, represented by a green color scale, and deposits represented by a red color scale. The calculated erosion volume is 327 cubic meters, and the volume of debris deposited is 533 cubic meters.

This highlights two different methods for estimating the volume of debris after a flooding event, depending on our data type and its quality. The median approach, as mentioned in Section 2.5.1, can be used when data has a large number of outliers, while the direct volume calculation approach, mentioned in Section 2.5.2, can be used in data without significant errors and outliers.

This method has certain sources of error, as in the median approach, it is assumed that all the pixels within a debris area share a constant height, which is the median height of a specific section. While this approach effectively removes extreme outliers, it may also generalize the actual data, potentially oversimplifying the variations. Additionally, this method is unable to account for the hidden debris located beneath the tree canopies.

Achieving high-precision volume estimates requires precisely georeferenced pre- and post-disaster images. In our case, accurately georeferenced LiDAR data would be the ideal choice for debris estimation. However, in the absence of such data, calculating differences at this fine scale remains a significant challenge.

Figure 22. Debris map of a section near the stream, from Figure 16, in Damascus. Here, the green section represents the eroded portion, and the red section represents deposits.

3.3. Flood Modeling in Damascus

Flood water depth in Damascus is estimated by performing simulations in HEC-RAS. The simulation takes approximately one hour on 32 GB of RAM and an i7 12th-gen processor for an area of six square km; however, configuring the simulation and collecting the data takes nearly one to two days.

Figure 23 shows the maximum water depth results for the flood event in Damascus. The color scale for the water depth is shown on the right of the image, with the maximum depth set to five meters.

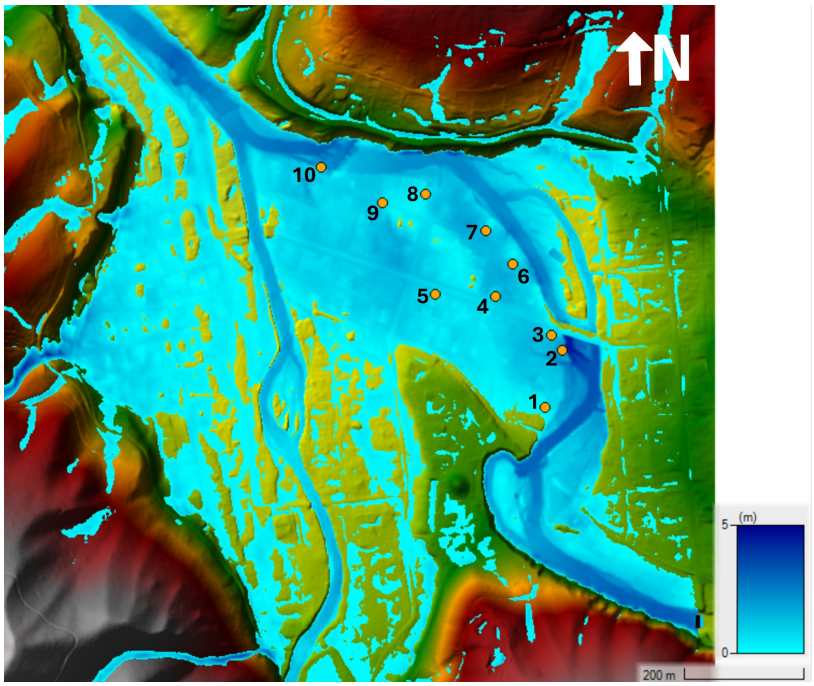

Figure 23. The HEC-RAS flood modeling results in Damascus, Virginia. Ten measurement locations are marked on the map, which are used to evaluate the accuracy of the results.

The water depth values determined by the calibrated HEC-RAS simulation are compared to the water depth values measured by the VDEQ. Table 5 shows a comparison of the results at the ten measurement locations highlighted in Figure 23.

Table 5. A comparison of measured water heights in Damascus and simulated water heights for ten locations.

Location	Measured Water Height (m)	Simulated Water Height (m)
1	0.64	0.64
2	1.80	1.82
3	1.27	1.21
4	0.89	0.94
5	0.28	0.53
6	1.02	1.07
7	0.64	0.65
8	0.79	0.66
9	0.84	0.84
10	1.85	1.82

Overall, the simulated water depth values are very accurate for this test area in Damascus. The major outlier is in the middle of the town at location five. The simulation result at this location is almost double the measured value that is provided to us. All but two of the measurement locations have an error of less than six percent, with multiple locations having errors of less than one percent. While a few locations result in a noticeable error, the water depth simulation appears to provide a very accurate representation of the flood event for the town of Damascus. The end-to-end flood height process error that includes the ground-truth measurements and modeling errors is 8%.

This level of accuracy of water depths further solidifies the use of the aforementioned Manning's coefficients from Whitehurst's dissertation for analyzing the flooding events in the Appalachian region. The simulated water depth can then be used to assess the flood impact on the buildings and further classify the damage as discussed in Section 1.

The validated water depth outputs are then used in the damage analysis using the methodology discussed in Section 2.5.4. For our sample data, the analyzed building types include RES1 (1 floor), RES1 (2 floors), and COM1, where RES and COM represent residential and commercial buildings, respectively. These categories are represented in Figure 19 by the colors red, orange, and blue, respectively. The specific positions in the legend correspond to their assigned classifications. Table 6 summarizes all the information used for these estimations and calculations of the final valuation loss.

Table 6. Property valuation loss as per depth–damage curve.

Building	Stories	Property Value ($)	Building Category	Flood Depth HEC-RAS (ft)	Damage Ratio (%)	Valuation Loss ($)
A	1	211,400	COM1	0.45–0.7	11.9–15.6	25,157–32,978
B	2	1,012,300	COM1	0.15–0.23	7.3–8.5	73,898–86,046
C	1.5	218,600	RES1, 2 floor	1.8–2.8	24–29	52,464–63,394
D	2	650,200	RES1, 2 floor	2.8–4.2	28.7–36	186,607–234,072
E	1	206,400	RES1, 1 floor	3–4.6	33.4–41.4	68,938–85,450
F	1.6	622,800	RES1, 2 floor	2–3	25–30	155,700–186,840

In Table 6, we show the range of valuation loss by applying the mean and standard deviation in % error to the flood depth. Using the range of flood water depth, the corresponding damage ratio can be identified from the graph in Figure 19. The damage ratio values beyond the least count of the graph are calculated from the slope of a small segment of the curve on which the required depth is present. It can be observed that the minimum and maximum values of the percent damage ratio and valuation loss do not differ by more than 31%.

4. Conclusions

This study developed a rapid, effective, and replicable methodology combining computer vision techniques, flood modeling, and GIS tools to estimate debris in lakes, land, and streams following a hurricane. By leveraging aerial imagery and advanced techniques, our approach provides actionable insights within the critical 72 h window after a disaster, facilitating informed decision-making by authorities.

For debris estimation in lakes, the integration of hybrid segmentation methods yielded results that can be converted to volume estimates closely aligned with the debris volumes reported by the DEQ. This method also provided more precise initial estimates compared to those provided by the USACE, demonstrating the utility of the hybrid approach in enhancing accuracy.

On land and near streams, utilizing DEMs generated from ODM provided critical insights into debris height and distribution. In particular, the integration of HEC-RAS flood modeling allowed us to refine the estimation process for building debris in Damascus. By incorporating FEMA's Hazus analysis-based tool and floodwater depth, our analysis provided a quick way to analyze building valuation loss. This refinement ensures that resource allocation is efficient.

Our approach can be easily replicated by anyone with training in GIS tools and HEC-RAS. For edge detection and color thresholding, users can use our code directly and change the edge thickness and color threshold range based on their debris characteristics. Additionally, segmentation in Roboflow requires no expertise, as the smart polygon tool segments the area with a single click.

The proposed methodologies represent a significant advancement in post-disaster debris assessment. They offer a quick and reliable way to quantify debris across multiple environments, significantly reducing the time and resources required for manual assessments. Furthermore, these techniques can be seamlessly integrated into disaster management workflows, enabling authorities to prioritize cleanup efforts, minimize environmental and economic impacts, and streamline recovery operations.

Author Contributions: Conceptualization, K.K., D.A. and D.W.; methodology, K.K.; software, D.A., S.G. and D.W.; validation, D.A. and D.W.; formal analysis, D.A., S.G. and D.W.; investigation, K.K.; resources, K.K.; data curation, D.A., S.G. and D.W.; writing—original draft preparation, K.K., D.A., D.W. and S.G.; writing—review and editing, K.K. and D.A.; visualization, D.A., S.G., and D.W.; supervision, K.K.; project administration, K.K. All authors have read and agreed to the published version of the manuscript.

Funding: This research received no external funding.

Data Availability Statement: The data presented in this study are available on request from the corresponding author.

Acknowledgments: We would like to thank the Virginia Department of Environmental Quality (DEQ) for their support and help with coordinating our data collection.

Conflicts of Interest: The authors declare no conflicts of interest.

Abbreviations

The following abbreviations are frequently used in this manuscript:

GIS	Geographic Information System
ODM	OpenDroneMap
UAV/UAS	Uncrewed Aerial Vehicle/System
DEM	Digital Elevation Model
PDA	Priliminary Damage Assessment

VDEQ/DEQ	Virginia Department of Environmental Quality
LiDAR	Light Detection and Ranging
Hazus	Hazards United States
HEC-RAS	Hydrologic Engineering Center's River Analysis System
USACE	U.S. Army Corps of Engineers
NRCS	Natural Resources Conservation Service
FEMA	Federal Emergency Management Agency
FAA	Federal Aviation Administration
SfM	Structure from Motion
HSV	Hue Saturation Value
RGB	Red Green Blue
AGL	Above Ground Level

References

1. Debris Removal Effort Ramps up at Claytor Lake with Additional Resources. Available online: https://www.nao.usace.army.mil/Media/News-Stories/Article/3948201/debris-removal-effort-ramps-up-at-claytor-lake-with-additional-resources/ (accessed on 21 January 2025).
2. Hurricane Rumor Response. Available online: https://www.fema.gov/disaster/recover/rumor/hurricane-rumor-response (accessed on 21 January 2025).
3. In the Wake of Hurricane Helene, Questions About Government Response Emerge. Available online: https://www.nbcnews.com/news/us-news/wake-hurricane-helene-questions-emerge-government-warnings-response-rcna173347 (accessed on 21 January 2025).
4. Sedighi, T.; Varga, L.; Hosseinian-Far, A.; Daneshkhah, A. Economic Evaluation of Mental Health Effects of Flooding Using Bayesian Networks. *Int. J. Environ. Res. Public Health* **2021**, *18*, 7467. [CrossRef] [PubMed]
5. Gourevitch, J.D.; Singh, N.K.; Minot, J.; Raub, K.B.; Rizzo, D.M.; Wemple, B.C.; Ricketts, T.H. Spatial targeting of floodplain restoration to equitably mitigate flood risk. *Glob. Environ. Change* **2020**, *61*, 102050. [CrossRef]
6. Sakurada, K.; Okatani, T.; Kitani, K.M. Hybrid macro–micro visual analysis for city-scale state estimation. *Comput. Vis. Image Underst.* **2016**, *146*, 86–98. [CrossRef]
7. Ghaffarian, S.; Kerle, N. Towards post-disaster debris identification for precise damage and recovery assessments from uav and satellite images. *Int. Arch. Photogramm. Remote Sens. Spat. Inf. Sci.* **2019**, *XLII-2/W13*, 297–302. [CrossRef]
8. Madkour, N.; Eren-Tokgoz, B.; Zhang, J.; Hwang, S.; Luo, Z. Debris Assessment for Waterways and Ports with Drone and Artificial Intelligence. *IISE Annu. Conf.* **2022**, 1–6.
9. Celik, T. Unsupervised Change Detection in Satellite Images Using Principal Component Analysis and *k*-Means Clustering. *IEEE Geosci. Remote Sens. Lett.* **2009**, *6*, 772–776. [CrossRef]
10. Simantiris, G.; Panagiotakis, C. Unsupervised Color-Based Flood Segmentation in UAV Imagery. *Remote Sens.* **2024**, *16*, 2126. [CrossRef]
11. Tamin, M.A.; Darwin, N.; Majid, Z.; Mohd Ariff, M.F.; Idris, K.M.; Manan Samad, A. Volume Estimation of Stockpile Using Unmanned Aerial Vehicle. In Proceedings of the 2019 9th IEEE International Conference on Control System, Computing and Engineering (ICCSCE), Penang, Malaysia, 29 November–1 December 2019; pp. 49–54. [CrossRef]
12. First Responder Beyond Visual Line of Sight. Available online: https://www.faa.gov/newsroom/fact_sheets/Fact_Sheet_BVLOS.pdf (accessed on 11 September 2025).
13. Rahnemoonfar, M.; Chowdhury, T.; Murphy, R. RescueNet: A High Resolution UAV Semantic Segmentation Dataset for Natural Disaster Damage Assessment. *Sci. Data* **2023**, *10*, 913. [CrossRef] [PubMed]
14. Rahnemoonfar, M.; Chowdhury, T.; Sarkar, A.; Varshney, D.; Yari, M.; Murphy, R. FloodNet: A High Resolution Aerial Imagery Dataset for Post Flood Scene Understanding. *arXiv* **2020**, arXiv:2012.02951. [CrossRef]
15. Nugraha, D.W.; Ilham, A.A.; Achmad, A.; Arief, A. Aerial imagery segmentation of natural disaster-affected areas using deep convolutional networks for disaster assessment. *AIP Conf. Proc.* **2024**, *2952*, 020001. [CrossRef]
16. Bekkaye, J.H.; Jafari, N.H. Flood Debris Quantification and Comparison Based on the Removal and Disposal Operation: Postdisaster Study of Beaumont, Texas Following Hurricane Harvey. *Nat. Hazards Rev.* **2023**, *24*, 05023008. [CrossRef]
17. NRCS Emergency Watershed Program. Available online: https://www.nrcs.usda.gov/programs-initiatives/ewp-emergency-watershed-protection (accessed on 25 January 2025).
18. FEMA Debris Estimating Field Guide. Available online: https://www.fema.gov/sites/default/files/2020-07/fema_329_debris-estimating_field-guide_9-1-2010.pdf (accessed on 7 December 2024).

19. NRCS Emergency Watershed Program Success Story. Available online: https://storymaps.arcgis.com/stories/140e557024ac42769ba3a7066600d8d8 (accessed on 25 January 2025).
20. Mantey, S.; Aduah, M. Comparative Analysis of Stockpile Volume Estimation using UAV and GPS Techniques. *Ghana Min. J.* **2021**, *21*, 1–10. [CrossRef]
21. Whitehurst, D.; Joshi, K.; Kochersberger, K.; Weeks, J. Post-Flood Analysis for Damage and Restoration Assessment Using Drone Imagery. *Remote Sens.* **2022**, *14*, 4952. [CrossRef]
22. Sattar, A.; Haritashya, U.; Kargel, J.; Karki, A. Transition of a small Himalayan glacier lake outburst flood to a giant transborder flood and debris flow. *Sci. Rep.* **2022**, *12*, 12421. [CrossRef] [PubMed]
23. Elkhrachy, I. Flash Flood Water Depth Estimation Using SAR Images, Digital Elevation Models, and Machine Learning Algorithms. *Remote Sens.* **2022**, *14*, 440. [CrossRef]
24. How a Disaster Gets Declared. Available online: https://www.fema.gov/disaster/how-declared (accessed on 25 January 2025).
25. FEMA PDA Pocket Guide. Available online: https://www.fema.gov/sites/default/files/documents/fema_rd_pda-pocket-guide_07012025.pdf (accessed on 25 January 2025).
26. Michaels, D.P. Developing a Rapid Assessment Procedure for the City of York. Available online: https://apps.usfa.fema.gov/pdf/efop/efo47605.pdf (accessed on 12 February 2025).
27. National Weather Service. National Water Center Products and Services. Available online: https://www.weather.gov/owp/operations (accessed on 20 July 2025).
28. NOAA National Severe Storms Laboratory. The Flooded Locations & Simulated Hydrographs Project. Available online: https://www.nssl.noaa.gov/projects/flash/ (accessed on 20 July 2025).
29. FEMA Hazus Analysis. Available online: https://www.fema.gov/flood-maps/products-tools/hazus (accessed on 25 January 2025).
30. OpenDroneMap. Drone Mapping Software. Available online: https://www.opendronemap.org/ (accessed on 18 November 2024).
31. Roboflow. Available online: https://roboflow.com/ (accessed on 14 November 2024).
32. Özyeşil, O.; Voroninski, V.; Basri, R.; Singer, A. A survey of structure from motion. *Acta Numer.* **2017**, *26*, 305–364. [CrossRef]
33. Schönberger, J.L.; Frahm, J.M. Structure-from-Motion Revisited. In Proceedings of the 2016 IEEE Conference on Computer Vision and Pattern Recognition (CVPR), Las Vegas, NV, USA, 27–30 June 2016; pp. 4104–4113. [CrossRef]
34. Bianco, S.; Ciocca, G.; Marelli, D. Evaluating the Performance of Structure from Motion Pipelines. *J. Imaging* **2018**, *4*, 98. [CrossRef]
35. OpenDroneMap Authors. ODM—A Command Line Toolkit to Generate Maps, Point Clouds, 3D Models and DEMs from Drone, Balloon or Kite Images. Available online: https://github.com/OpenDroneMap/ODM (accessed on 18 November 2024).
36. Yang, X.; Li, J. (Eds.) *Advances in Mapping from Remote Sensor Imagery: Techniques and Applications*, 1st ed.; CRC Press: Boca Raton, FL, USA, 2013. [CrossRef]
37. He, K.; Gkioxari, G.; Dollár, P.; Girshick, R. Mask R-CNN. *arXiv* **2018**, arXiv:1703.06870. [PubMed]
38. Kirillov, A.; Mintun, E.; Ravi, N.; Mao, H.; Rolland, C.; Gustafson, L.; Xiao, T.; Whitehead, S.; Berg, A.C.; Lo, W.Y.; et al. Segment Anything. *arXiv* **2023**, arXiv:2304.02643. [PubMed]
39. Lin, T.Y.; Maire, M.; Belongie, S.; Bourdev, L.; Girshick, R.; Hays, J.; Perona, P.; Ramanan, D.; Zitnick, C.L.; Dollár, P. Microsoft COCO: Common Objects in Context. *arXiv* **2015**, arXiv:1405.0312. [CrossRef]
40. Segment Anything. Research by Meta AI. Available online: https://segment-anything.com/demo (accessed on 18 November 2024).
41. Roboflow. Smart Polygon (AI Labeling). Available online: https://docs.roboflow.com/annotate/use-roboflow-annotate/smart-polygon (accessed on 14 November 2024).
42. HEC-RAS. Available online: https://www.hec.usace.army.mil/software/hec-ras/ (accessed on 15 November 2024).
43. Virginia LiDAR Download Application. Available online: https://vgin.vdem.virginia.gov/apps/VGIN::virginia-lidar-download-application/explore (accessed on 18 November 2024).
44. Dewitz, J. National Land Cover Database (NLCD) 2021 Products. 2023. Available online: https://www.sciencebase.gov/catalog/item/647626cbd34e4e58932d9d4e (accessed on 18 November 2024).
45. USACE Hydrologic Engineering Center. Creating Land Cover, Manning's n Values, and % Impervious Layers. Available online: https://www.hec.usace.army.mil/confluence/rasdocs/r2dum/6.6/developing-a-terrain-model-and-geospatial-layers/creating-land-cover-mannings-n-values-and-impervious-layers (accessed on 18 November 2024).
46. Whitehurst, D.S. Aerial Cadastral and Flood Assessment for Disaster Risk Management in Appalachia. Ph.D. Dissertation, Virginia Polytechnic Institute and State University, Blacksburg, VA, USA, 2023.
47. NSSL Projects: Multi-Radar/Multi-Sensor System (MRMS). Available online: https://www.nssl.noaa.gov/projects/mrms/ (accessed on 23 October 2024).
48. Washington County Geospatial Web Portal. Available online: https://www.washcova.com/data-and-map-requests/ (accessed on 25 January 2025).

49. HAZUS Flood Model Technical Manual. Available online: https://www.fema.gov/sites/default/files/documents/fema_hazus-flood-model-technical-manual-6-1.pdf (accessed on 25 January 2025).
50. NSF NHERI SimCenter. Available online: https://nheri-simcenter.github.io/R2D-Documentation/common/testbeds/atlantic_city/damage_and_loss.html (accessed on 25 January 2025).